

1   **A New Method for Calculating Number Concentrations of Cloud  
2   Condensation Nuclei Based on Measurements of A Three-wavelength  
3   Humidified Nephelometer System**

4   Jiangchuan Tao<sup>1</sup>, Chunsheng Zhao<sup>1</sup>, Ye Kuang<sup>1</sup>, Gang Zhao<sup>1</sup>, Chuanyang Shen<sup>1</sup>, Yingli Yu<sup>1</sup>, Yuxuan  
5   Bian<sup>2</sup>, Wanyun Xu<sup>2</sup>

6   [1]{Department of Atmospheric and Oceanic Sciences, School of Physics, Peking University, Beijing,  
7   China}

8   [2]{State Key Laboratory of Severe Weather, Chinese Academy of Meteorological Sciences}

9   \*Correspondence to: C. S. Zhao (zcs@pku.edu.cn)

10   Abstract

11         The number concentration of cloud condensation nuclei (CCN) plays a fundamental role in  
12         cloud physics. Instrumentations of direct measurements of CCN number concentration ( $N_{CCN}$ ) based  
13         on chamber technology are complex and costly, thus a simple way for measuring  $N_{CCN}$  is needed. In  
14         this study, a new method for  $N_{CCN}$  calculation based on measurements of a three-wavelength  
15         humidified nephelometer system is proposed. A three-wavelength humidified nephelometer system  
16         can measure aerosol light scattering coefficient ( $\sigma_{sp}$ ) at three wavelengths and the light scattering  
17         enhancement factor (fRH). The Angstrom exponent ( $\text{\AA}$ ) inferred from  $\sigma_{sp}$  at three wavelengths  
18         provides information on mean predominate aerosol size and hygroscopicity parameter ( $\kappa$ ) can be  
19         calculated from the combination of fRH and  $\text{\AA}$ . Given this, a look-up table that involves  $\sigma_{sp}$ ,  $\kappa$  and  
20          $\text{\AA}$  is established to predict  $N_{CCN}$ . Due to the precondition for the application, this new method is not  
21         suitable for externally mixed particles, large particles (e.g. dust and sea salt) or particles near single  
22         source regions. This method is validated with direct measurements of  $N_{CCN}$  using a CCN counter on  
23         the North China Plain. Results show that relative deviations between calculated  $N_{CCN}$  and measured  
24          $N_{CCN}$  are within 30% and confirm the robustness of this method. This method enables simpler  $N_{CCN}$   
25         measurements because the humidified nephelometer system is easily operated and stable. Compared

26 with the method of CCN counter, another advantage of this newly proposed method is that it can  
27 obtain  $N_{CCN}$  at lower supersaturations in the ambient atmosphere.  
28

29 1. Introduction

30 Cloud condensation nuclei (CCN) is the aerosol particle forming cloud droplet by hygroscopic  
31 growth. CCN number concentration ( $N_{CCN}$ ) plays a fundamental role in cloud micro physics and  
32 aerosol indirect radiative effect. In general, the direct measurement of  $N_{CCN}$  is achieved in a cloud  
33 chamber under super-saturated conditions (Hudson, 1989; Nenes et al., 2001; Rose et al., 2008). Due  
34 to the requirement of high accuracies of working conditions like temperatures, vapors and flow rates  
35 in cloud chambers, the direct measurement of  $N_{CCN}$  is complex and costly (Rose et al., 2008; Lathem  
36 and Nenes, 2011). Thus, developments of simplified measurements of  $N_{CCN}$  are required. In recent  
37 years, attention has been focused on measurements of aerosol optical properties (Jefferson,  
38 2010; Ervens et al., 2007; Gasso and Hegg, 2003), which are simple and well-developed (Covert et al.,  
39 1972; Titos et al., 2016). For aerosol population free of sea salt or dust, the accumulation mode  
40 aerosol not only dominates aerosol scattering ability but also contribute most to  $N_{CCN}$ . Thus, the  
41 calculation of  $N_{CCN}$  based on measurements of aerosol optical properties is feasible, and can facilitate  
42  $N_{CCN}$  measurement.

43 There are two kinds of methods to calculating  $N_{CCN}$  based on measurements of aerosol optical  
44 properties. For the first kind,  $N_{CCN}$  as well as the hygroscopicity parameter ( $\kappa$ ) can be calculated  
45 based on measurements of a humidified nephelometer system in combination with aerosol particle  
46 number size distribution (PNSD) (Ervens et al., 2007; Chen et al., 2014). Thus additional  
47 measurements of PNSD are needed. For the second kind,  $N_{CCN}$  is calculated based on statistical  
48 relationships between  $N_{CCN}$  and aerosol optical properties, such as scattering coefficient ( $\sigma_{sp}$ ),  
49 Angstrom Exponent ( $\text{\AA}$ , which is the exponent commonly used to describe the dependence of  $\sigma_{sp}$  on  
50 wavelength) and single scattering albedo (SSA) (Jefferson, 2010; Shinozuka et al., 2015). Compared  
51 with the first kind, whose  $R^2$  can be about 0.9, instruments used in the second kind of methods are  
52 cheaper and easier in operation, but has a lower accuracy of  $R^2$  much lower than 0.9. Applications  
53 similar to the second kind are widely used in remote sensing. As shown in Table 1, earlier studies

54 found that the aerosol volume or aerosol PNSD retrieved from remote sensing measurements can be  
55 used to calculate  $N_{CCN}$  (Gasso and Hegg, 2003;Kapustin et al., 2006). Recently, aerosol optical depth  
56 (AOD) or aerosol vertical profile is used to predict  $N_{CCN}$  directly(Ghan and Collins, 2004;Ghan et al.,  
57 2006;Andreae, 2009;Liu and Li, 2014).

58 In the statistical relationship between  $N_{CCN}$  and aerosol optical properties,  $\sigma_{sp}$  or AOD is mainly  
59 the proxy of aerosol absolute concentration, while Å or SSA can be used to reveal the variations of  
60 aerosol CCN activity, as shown in Table 1. Based on Kohler theory (Köhler, 1936;Petters and  
61 Kreidenweis, 2007), aerosol CCN activity is determined by aerosol size and aerosol chemical  
62 composition which is defined as aerosol hygroscopicity. Information about aerosol size and aerosol  
63 hygroscopicity are critical to  $N_{CCN}$  prediction and their absence can lead to a deviation with factor of  
64 four (Andreae, 2009). Compared with aerosol hygroscopicity, aerosol size is more important in  
65 determining CCN activity (Dusek et al., 2006). The value of Å can provide information on mean  
66 predominate aerosol size (Brock et al., 2016;Kuang et al., 2017a). As a result,  $N_{CCN}$  calculation from  
67 Å and extinction coefficient is found to be accurate to some extent (Shinozuka et al., 2015). As  
68 proxies for aerosol hygroscopicity, SSA or aerosol light scattering enhancement factor (fRH) is  
69 commonly used while not so effective (Jefferson, 2010; Liu and Li, 2014). SSA is determined by the  
70 ratio between the light absorbing carbonaceous and less-absorbing components. Black carbon  
71 dominates the absorption of solar radiation and is a main hydrophobic composition as well.  
72 Less-absorbing components consist of inorganic salts and acids, as well as most organic compounds,  
73 which are generally hygroscopic compositions. SSA correlates positively with aerosol hygroscopicity  
74 (Rose et al., 2010) but deviates significantly due to the diversity of hygroscopicity of less-absorbing  
75 components. Thus  $N_{CCN}$  calculation combining SSA, backscatter fraction and  $\sigma_{sp}$  still lead to  
76 significant deviations, with a 0.6  $R^2$  (Jefferson, 2010). As for fRH, there was a study applied aerosol  
77 optical quantities ( $\sigma_{sp}$  or aerosol optical thickness) with fRH or SSA to calculate  $N_{CCN}$  (Liu and Li,  
78 2014). In their study, compared with the combination of SSA and aerosol optical quantities, the  
79 combination of fRH and aerosol optical quantities is found to be less effective in estimating  $N_{CCN}$ ,  
80 even though fRH directly connected with aerosol hygroscopicity (Liu and Li, 2014). This may result  
81 from the significant dependence of fRH on aerosol size(Chen et al., 2014;Kreidenweis and

82 Asa-Awuku, 2014;Kuang et al., 2017a). As mentioned before, PNSD is used for better calculation of  
83  $\kappa$  and  $N_{CCN}$  from fRH in previous studies (Ervens et al., 2007;Chen et al., 2014). A new method to  
84 estimate  $\kappa$  from fRH and  $\text{\AA}$  was proposed recently (Kuang et al., 2017a;Brock et al., 2016). Based  
85 on this method, fRH can be used to calculate  $N_{CCN}$  without measurements of PNSD and can be  
86 expected to improve the  $N_{CCN}$  prediction just based on measurements of aerosol optical properties.

87 In this study, the relationship between  $N_{CCN}$  and aerosol optical properties measured by a  
88 humidified nephelometer system is studied and a new method for  $N_{CCN}$  prediction is proposed. This  
89 new method is validated based on data observed in Gucheng campaign on the North China Plain and  
90 can be expected to improve measurements of  $N_{CCN}$  due to advantages of applying nephelometers.

91

## 92 2. Methodology

### 93 2.1. Data

94 Data in this study are mainly measured at Gucheng (39.15N, 115.74E) during autumn in 2016  
95 on the North China Plain (NCP). Gucheng is 100km southwest from Beijing and 40km northeast  
96 from Baoding under background pollution condition in the NCP. The observation site was  
97 surrounded by farmland and about 3km away from the Gucheng town. This campaign started on 20  
98 October and lasted for nearly one month.

99 Instruments used in Gucheng campaign were located in a measurement container under  
100 temperature maintained at 25 °C. Ambient aerosol was sampled and dried to relative humidity (RH)  
101 lower than 30% by an inlet system consisting of a PM10 inlet, an inline Nafion dryers and a RH and  
102 temperature sensor (Vaisala HMP110). Then the sample aerosol was separated by a splitter and  
103 directed into various instruments. During this campaign, aerosol scattering coefficient ( $\sigma_{sp}$ ), aerosol  
104 optical hygroscopic growth factor (fRH), particle size-resolved activation ratio (AR) and particle  
105 number size distribution (PNSD) were obtained.

106 fRH as well as  $\sigma_{sp}$  at three wavelengths were measured by a humidified nephelometer system  
107 consisting of two nephelometers (Aurora 3000, Ecotech Inc.) and a humidifier.  $\sigma_{sp}$  can be described  
108 by a formula of  $\text{\AA}$ :

109

$$\sigma_{sp}(\lambda) = \beta \cdot \lambda^A, \quad (1)$$

110 where  $\beta$  is the aerosol number concentration and  $\lambda$  is the wavelength. Thus  $\text{\AA}$  can be calculated  
111 directly from  $\sigma_{sp}$  measured by a nephelometer. The humidifier with a Gore-Tex tube humidified the  
112 sample air up to 90% RH. A whole cycle of humidification lasted about 45 minutes from 50% RH to  
113 90% RH. Dried  $\sigma_{sp}$  was obtained directly from dried sample aerosol measured by one nephelometer  
114 and humidified  $\sigma_{sp}$  was obtained from humidified aerosol measured by another nephelometer.  $fRH$   
115 is defined as:

116

$$fRH = \sigma_{sp}(RH)/\sigma_{sp} \quad (2)$$

117 where  $\sigma_{sp}(RH)$  is the humidified  $\sigma_{sp}$  at each RH. Detailed description of the humidified  
118 nephelometer system was illustrated in Kuang et al (2017a).

119 The particle size-resolved activation ratio (AR), defined as the ratio of  $N_{CCN}$  to total particles,  
120 was measured by a system mainly consisting of a differential mobility analyzer (DMA, Model 3081)  
121 and a continuous-flow CCN counter (model CCN200, Droplet Measurement Technologies, USA;  
122 Roberts and Nenes (2005);;Lance et al.,(2006)). The system selected mono-disperse particles with  
123 the DMA coupled with an electrostatic classifier (model 3080; TSI, Inc., Shoreview, MN USA) and  
124 measured AR of the mono-disperse particles by a condensation particle counter (CPC model 3776;  
125 TSI, Inc.) and CCN counter. Ranges of particle size and supersaturation were 10-300nm and  
126 0.07%-0.80%, respectively. Measurements at five supersaturations (0.07%, 0.10%, 0.20%, 0.40%  
127 and 0.80%) were conducted sequentially with each cycle lasted for 1 hour, and  $N_{CCN}$  at 0.07%  
128 supersaturation was used in this study. Before and after the campaign, supersaturations set in this  
129 system were calibrated using ammonium sulfate (Rose et al., 2008). More information about the  
130 system are given in Deng et al. (2011) and Ma et al.(2016).

131 PNSD with particle diameter from 9nm to 10um was measured by a mobility particle size  
132 spectrometer (SMPS, TSI Inc., Model 3996) and an Aerodynamic Particle Sizer (APS, TSI Inc.,  
133 Model 3321). SMPS consisted of a DMA, an electrostatic classifier and a CPC (model 3776; TSI,  
134 Inc., Shoreview, MN USA) and measured PNSD with diameter lower than 700nm.

135 In addition, PNSD and  $\sigma_{sp}$  from 2011 to 2014 at four campaigns (Wuqing in 2011, Xianghe in

136 2012 and 2013, and Wangdu in 2014) in NCP were used in this study. PNSD in these campaigns was  
137 measured by a Twin Differential Mobility Particle Sizer (TDMPS, Leibniz-Institute for Tropospheric  
138 Research (IfT), Germany) and an Aerodynamic Particle Sizer (APS, TSI Inc., Model 3321). A TSI  
139 3563 nephelometer was used to obtain  $\sigma_{sp}$  at three wavelengths. Details about the four campaigns  
140 can be found in Ma et al. (2011), Ma et al.(2016), Kuang et al. (2016) and Kuang et al.(2017a).

141

142 2.2. Theories

143 Hygroscopic growth of particles at certain relative humidity can be described by  $\kappa$ -Köhler  
144 theory (Petters and Kreidenweis, 2007):

145 
$$\frac{RH}{100} = \frac{g(RH)^3 - 1}{g(RH)^3 - (1-\kappa)} \cdot \exp\left(\frac{4\sigma_{s/a} \cdot M_w}{R \cdot T \cdot D_d \cdot g \cdot \rho_w}\right) \quad (1)$$

146 where  $g(RH)$  is geometric diameter growth factor,  $\kappa$  is the hygroscopicity parameter, RH is the  
147 relative humidity;  $\rho_w$  is the density of water;  $M_w$  is the molecular weight of water;  $\sigma_{s/a}$  is the surface  
148 tension of the solution-air interface, which is assumed to be equal to the surface tension of the pure  
149 water-air interface; R is the universal gas constant; and T is the temperature.

150 Accounting for the impact of  $\text{\AA}$ ,  $\kappa_f$  can be derived directly from fRH (Brock et al., 2016;Kuang  
151 et al., 2017a). A single-parameter parameterization scheme proposed by Brock et al. (2016) connects  
152 fRH and  $\kappa$  by the approximately proportional relationship between total aerosol volume and  $\sigma_{sp}$ :

153 
$$f(RH) = 1 + \kappa_{sca} * RH / (100 - RH) \quad (2)$$

154 where  $\kappa_{sca}$  is a parameter for fitting fRH curves and is found can be used to predict  $\kappa_f$  in  
155 combination wih  $\text{\AA}$  in recent studies (Brock et al., 2016;Kuang et al., 2017a). This method of  
156 calculating  $\kappa_f$  based on  $\kappa_{sca}$  and  $\text{\AA}$  was confirmed by good agreement with  $\kappa_f$  calculated from  
157 fRH and PNSD.

158  $N_{CCN}$  can be calculated from size-resolved AR at a certain supersaturation (SS) and PNSD  
159 (referred to as  $n(\log D_p)$ ) as follows:

160 
$$N_{CCN} = \int_{\log D_p} AR(\log D_p, SS) \cdot n(\log D_p) d \log D_p \quad (3)$$

161 In general, size-resolved AR curves are complicated and always replaced by a critical diameter to  
162 simplify calculation (Deng et al., 2013). The critical diameter is defined as:

163 
$$N_{CCN} = \int_{\log D_c}^{\log D_{P,max}} n(\log D_p) d \log D_p \quad (4)$$

164 where  $D_{P,max}$  is the maximum diameter of the measured particle number size distribution. In other  
165 words, the integral of PNSD larger than  $D_c$  equals to the measured  $N_{CCN}$ . And a critical  $\kappa$  ( $\kappa_c$ ) can be  
166 calculated by equation (1) and indicates CCN activity and hygroscopicity of particles.

167

### 168 3. Results

#### 169 3.1. Calculation of $N_{CCN}$ based on measurements of a Humidified Nephelometer system

170 Free of sea salt aerosol and dust aerosol, accumulation mode aerosol dominates both the optical  
171 scattering ability at short wavelengths and the CCN activity at low supersaturations, and thus a  
172 reasonable relationship between  $\sigma_{sp}$  and  $N_{CCN}$  can be achieved. Figure 1 shows the size distribution  
173 of cumulative contributions of  $\sigma_{sp}$  at 450nm and  $N_{CCN}$  at 0.07% with various Å and  $\kappa_c$ , and  
174 corresponding normalized PNSDs based on data measured at the four campaigns on the North China  
175 Plain. During the four campaigns, no sea salt aerosol or dust aerosol was observed(Ma et al.,  
176 2011;Ma et al., 2016;Kuang et al., 2016;Kuang et al., 2017a). For continental aerosol without sea salt  
177 or dust, Å varies from 0.5 to 1.8 and  $\kappa_c$  varies from 0.1 to 0.5 (Cheng et al., 2008;Ma et al.,  
178 2011;Liu et al., 2014;Kuang et al., 2017b). And as mentioned before, Å can be used as a proxy of  
179 the overall size distribution of aerosol populations, with smaller Å indicating more larger particles.  
180 In figure 1, comparisons for Å are made between 0.5 and 1.9 and for  $\kappa_c$  are made between 0.1 and  
181 0.5. As larger particles contribute more to light scattering and activation, cumulative contributions of  
182 both  $\sigma_{sp}$  and  $N_{CCN}$  increase significantly at the diameter range of accumulation mode particles.  
183 Because more hygroscopic particles are able to activate at smaller diameters, the cumulative  
184 contribution of  $N_{CCN}$  with higher  $\kappa_c$  increases at smaller diameters. In general, major contributions  
185 of both  $\sigma_{sp}$  and  $N_{CCN}$  are made by particles from 200nm to 500nm for various Å and  $\kappa_c$ . This  
186 implies the feasibility of inferring  $N_{CCN}$  from aerosol optical properties.

187 Because particles smaller than 200nm can activate at supersaturations higher than 0.07% while  
188 scatter less light at wavelengths longer than 450nm, which are shown as the light color lines in  
189 Figure 1, it's obvious that significant differences will exist between cumulative contributions of  $\sigma_{sp}$   
190 and  $N_{CCN}$ . This means  $\sigma_{sp}$  and  $N_{CCN}$  are dominated by different particles and poor correlation  
191 between  $\sigma_{sp}$  and  $N_{CCN}$  can be expected. Thus the method of inferring  $N_{CCN}$  from aerosol optical  
192 properties is applicable for shorter wavelength and lower supersaturations.

193 Furthermore, PNSD with higher Å indicates more Aitken mode particles and fewer  
194 accumulation mode particles. Thus large particles contribute less for both  $\sigma_{sp}$  and  $N_{CCN}$  when Å are  
195 higher, characterizing an increase of cumulative contribution curves at smaller diameters. In detail,  
196 differences of cumulative contribution curves between 0.5 Å and 1.9 Å are about 150nm for  $\sigma_{sp}$   
197 and about 100nm for  $N_{CCN}$ , by estimating the average of differences of diameters where cumulative  
198 contributions range from 0.2 to 0.8. Changes of cumulative contributions of  $N_{CCN}$  and  $\sigma_{sp}$  with  
199 various Å reveal that the shape of PNSD can influence the correlation between  $N_{CCN}$  and  $\sigma_{sp}$ . This  
200 is confirmed by previous studies in which the Å is found to play an important role in calculating  
201  $N_{CCN}$  from  $\sigma_{sp}$  (Shinozuka et al., 2015; Liu and Li, 2014).

202 The relationship between  $\sigma_{sp}$  and  $N_{CCN}$  dependent on Å and  $\kappa_c$  is evaluated by calculating  
203  $\sigma_{sp}$  and  $N_{CCN}$  with different PNSDs (classified by Å) and different  $\kappa_c$ . In detail, ratios of  $N_{CCN}$  to  
204  $\sigma_{sp}$ , referred to as  $AR_{sp}$ , are calculated to eliminate the effect of variations of particle concentrations  
205 consistent at all diameters. Results at the supersaturation of 0.07% are shown in figure 2 and  $AR_{sp}$  is  
206 higher than 0 and lower than 10. In general,  $AR_{sp}$  are higher for more hygroscopic particles or  
207 smaller particles. As particles become more hygroscopic, more CCN can be expected when  $\sigma_{sp}$  is  
208 fixed. As aerosol populations consist of more smaller CCN-active particles, the increase of  $\sigma_{sp}$  is  
209 weaker than that of  $N_{CCN}$ . For example, paticles with diameters slightly larger than  $D_c$  contribute less  
210 to  $\sigma_{sp}$  than paticles with diameters much larger than  $D_c$ .

211 In detail, the sensitivity of  $AR_{sp}$  to  $\text{\AA}$  also changes with  $\text{\AA}$  and  $\kappa_c$ . When  $\text{\AA}$  are higher than 1.4  
212 and  $\kappa_c$  is lower than 0.2,  $AR_{sp}$  is insensitive to  $\text{\AA}$ . While when  $\text{\AA}$  are lower than 1 and  $\kappa_c$  are  
213 higher than about 0.3,  $AR_{sp}$  is more sensitive to  $\text{\AA}$  than  $\kappa_c$ . This higher sensitivity of  $AR_{sp}$  to  $\text{\AA}$   
214 reveals that particles having mean predominate size smaller than existing particles can contribute  
215 more to  $N_{CCN}$ . This is the consequence of the sensitivity of  $AR_{sp}$  to  $\text{\AA}$  resulting from the variation of  
216 small CCN-active particles, as mentioned before.

217 Based on the lookup-table illustrated in Figure 2,  $N_{CCN}$  at the supersaturation of 0.07% can be  
218 calculated simply from  $\text{\AA}$ ,  $\kappa_f$  and  $\sigma_{sp}$  which can be obtained from measurements of a humidified  
219 nephelometer system. The description of this simple method is shown in figure 3. A new look-up  
220 table needs to be made for  $N_{CCN}$  estimation at other supersaturations, which should better be less than  
221 0.07% as mentioned in the discussion of figure 1.

222 One critical issue about the method is the conversion of the  $\kappa_f$  obtained from the humidified  
223 nephelometer system to the  $\kappa_c$  under super-saturated conditions. There are mainly two factors  
224 making this conversion necessary. First, closure studies of aerosol hygroscopicity found significant  
225 deviations between hygroscopicity at sub-saturated conditions and super-saturated conditions (Wex  
226 et al., 2009; Irwin et al., 2010; Good et al., 2010; Renbaum-Wolff et al. 2016). Their difference can  
227 be expected to be about 0.1 for accumulation mode aerosol(Wu et al., 2013;Whitehead et al.,  
228 2014;Ma et al., 2016). Second,  $\kappa_f$  indicates the hygroscopicity of total particles and can be quite  
229 different from aerosol hygroscopicity at a specific diameter due to variations of size-dependent  
230 particle hygroscopicity. Kuang et al. (2017a) found a difference around 0.1 between  $\kappa_f$  and  $\kappa$   
231 inferred from g(RH) measurements for accumulation mode particles whose  $\kappa_f$  is no larger than 0.2.  
232 In this study, a simple conversion that  $\kappa_c$  is 0.2 higher than  $\kappa_f$  is used to calculate  $N_{CCN}$ , while for  
233  $\kappa_f$  larger than 0.2, a smaller difference of 0.1 between  $\kappa_c$  and  $\kappa_f$  should be used (Kuang et al.,  
234 2017a). This simplified relationship between  $\kappa_c$  and  $\kappa_f$  is a rough estimate regardless of the  
235 complexity of differences of aerosol hygroscopicity measured by different instruments, but still used  
236 in this study for two reasons. First, the accurate conversion cannot be achieved without detailed  
237 information of the particle hygroscopicity, which is difficult and complicated to measure. Second, a  
238 deviation of  $\kappa_c$  less than 0.1 generally leads to a deviation of  $N_{CCN}$  less than 20% (Ma et al., 2016),  
239 which is comparable with the deviation of CCN measurements. As a result, for a simple method of

240  $N_{CCN}$  calculation, this conversion is quite easy. In addition, it is important to note that the value of the  
241 difference between  $\kappa_c$  and  $\kappa_f$  is also a rough estimate regardless of the complexity of aerosol  
242 hygroscopicity under different conditions, and the influence of  $\Delta\kappa$  deviation on  $N_{CCN}$  calculation  
243 needs to be further examined based on field observation. In regions of single aerosol emissions or  
244 productions, the actual  $\Delta\kappa$  can be too large (some organic compositions, Wex et al., 2009;  
245 Renbaum-Wolff et al., 2016) or too small (inorganic compositions and black carbon) and thus is not  
246 suitable for the application of this method.

247 Besides aerosol size and hygroscopicity, aerosol mixing state can also affect aerosol cloud  
248 activity. When primary aerosol emissions are strong, aerosol populations are likely to be externally  
249 mixed and a realistic treatment of aerosol mixing state is critical for  $N_{CCN}$  calculation (Cubison et al.,  
250 2008;Wex et al., 2010). But for regions away from strong aerosol primary emissions, the influence of  
251 mixing state on aerosol cloud activity is small and the assumption of internal mixing state is effective  
252 for the estimation of  $N_{CCN}$  (Dusek et al., 2006;Deng et al., 2013;Ervens et al., 2010). For regions  
253 above the boundary layer where clouds form and measurements of  $N_{CCN}$  are important, this  
254 conclusion is tenable if there are no plumes(Moteki and Kondo, 2007;McMeeking et al., 2011). In  
255 the new method of this paper aerosol populations are assumed to be internally mixed. Thus this  
256 method might not be applicable for regions or air masses greatly affected by strong primary aerosol  
257 emissions. Furthermore, this new method cannot be applied for regions where sea salt or dust  
258 prevails, as mentioned before. In summary, this method can be used to calculate  $N_{CCN}$  for continental  
259 regions, especially at clouds forming heights, where aged aerosol particles dominate.

260 3.2. Validation based on  $N_{CCN}$  measurement

261 The method for calculating  $N_{CCN}$  based on measurement of the humidified nephelometer system,  
262 including the conversion of  $\kappa_c$  and the lookup-table, is examined using data measured in Gucheng.

263 Overview of data in Gucheng is shown in Figure 4. From polluted periods to clean periods,  
264 significant variations of  $N_{CCN}$  and  $\sigma_{sp}$  can be found but AR<sub>sp</sub> of  $N_{CCN}$  to  $\sigma_{sp}$  stays around 5. On  
265 October 23<sup>rd</sup> and 29<sup>th</sup>,  $N_{CCN}$  and  $\sigma_{sp}$  are lower than 2000#/cm<sup>3</sup> and 500Mm<sup>-1</sup>, respectively. While on  
266 October 20<sup>th</sup>, 26<sup>th</sup> and November 3<sup>rd</sup>,  $N_{CCN}$  and  $\sigma_{sp}$  are higher than 2000#/cm<sup>3</sup> and 500Mm<sup>-1</sup>,

267 respectively. These variations of  $N_{CCN}$  and  $\sigma_{sp}$  are mainly due to the variation of the particle number  
268 concentration rather than the shape of particle size distribution and aerosol hygroscopicity. Variations  
269 of  $AR_{sp}$  result from the variations of  $\text{\AA}$  and  $\kappa_c$ , which indicate the variations of aerosol  
270 microphysical properties and chemical compositions.

271 In general,  $AR_{sp}$  is more sensitive to variations of  $\text{\AA}$  than  $\kappa_c$ . As mentioned before, the  
272 sensitivity of  $AR_{sp}$  to  $\text{\AA}$  is determined by both  $\text{\AA}$  and  $\kappa_f$ . In detail,  $\text{\AA}$  during the campaign mainly  
273 ranges from 0.5 to 1.5 and  $\kappa_f$  ranges mainly from 0.05 to 0.2, which means that  $\kappa_c$  ranges from  
274 0.25 to 0.4. These values of  $\text{\AA}$  and  $\kappa_f$  correspond a significant sensitivity of  $AR_{sp}$  to  $\text{\AA}$ , as the  
275 lookup table shows in figure 2. The sensitivity of  $AR_{sp}$  to  $\kappa_c$  is much small and only notable during  
276 some short periods (grey bars in Figure 4). For example, from November 5<sup>th</sup> to 7<sup>th</sup>, variations of  $\kappa_f$   
277 and  $\text{\AA}$  are opposite and result in nearly constant  $AR_{sp}$ . And from October 30<sup>th</sup> to November 2<sup>nd</sup>,  
278 consistent variations of  $\text{\AA}$  and  $\kappa_f$  lead to greater variations of  $AR_{sp}$  than other periods. This weak  
279 sensitivity of  $AR_{sp}$  to  $\kappa_f$  may be due to the uncertainty of  $\kappa_c$  calculated from  $\kappa_f$  based on the  
280 simplified conversion.

281 This simplified conversion of  $\kappa_c$  is examined by comparing  $\kappa_f$  and  $\kappa_c$  measured in Gucheng  
282 campaign, shown in Figure 5. In general,  $\Delta\kappa$  that indicates the difference between  $\kappa_f$  and  $\kappa_c$  is  
283 around 0.2 and independent from  $\text{\AA}$  and  $\kappa_c$ . Over 80% of  $\Delta\kappa$  ranges from 0.1 to 0.3 that confirms  
284 applicability of the simplified conversion of  $\kappa_c$ . However, a notable deviation of  $\Delta\kappa$  can be found  
285 when  $\text{\AA}$  is higher than 1.5. High values of  $\text{\AA}$  represent existence of small particles. Compositions  
286 and mixing state of these small particles, which may be fresh emitted and experience inefficient  
287 aging processes, are diverse and likely to deviate from the simplified conversion of  $\kappa_c$ .

288 Therefore, considering the deviation of  $\kappa_c$  conversion and high sensitivity of  $AR_{sp}$  to  $\kappa_c$  when  
289  $\text{\AA}$  is higher than 1.5, the method of calculating  $N_{CCN}$  from measurements of a humidified  
290 nephelometer system may lead to significant deviation in this case which means that this method can  
291 only be adopted when  $\text{\AA}$  is lower than 1.5.

292 Based on the lookup table of  $\kappa_c$  and  $\text{\AA}$ ,  $AR_{sp}$  is calculated and applied to calculate  $N_{CCN}$  with  
293  $\sigma_{sp}$ . The calculated  $AR_{sp}$  and  $N_{CCN}$  are compared with the measured  $AR_{sp}$  and  $N_{CCN}$  shown as the  
294 green dots in Figure 6. In general, good agreements between calculations and measurements are

achieved and relative deviations are within 30%. For the comparison of  $AR_{sp}$ , the system relative deviation is less than 10%. For the comparison of  $N_{CCN}$ , the slope and the correlation coefficient of the regression are 1.03 and 0.966, respectively.

In addition, the influence of the  $\kappa_c$  conversion on  $AR_{sp}$  and  $N_{CCN}$  calculation are evaluated in two ways. In the first way,  $\Delta\kappa$  of the  $\kappa_c$  conversion is set to be 0.05 higher or lower, which means  $\Delta\kappa$  of 0.25 or 0.15. The corresponding results are presented as the red dots and blue dots in Figure 6. In the second way, a constant  $\kappa_c$  of 0.34, which is the average of  $\kappa_c$  values in Gucheng campaign, is used to calculate  $AR_{sp}$  and  $N_{CCN}$ , and shown as the grey dots in Figure 6. In general, differences among calculations using various  $\kappa_c$  conversions are quite small. The  $\Delta\kappa$  difference of 0.05 in  $\kappa_c$  conversion only leads to a difference of 10% for the system relative deviation. The correlation coefficient of the calculation using a constant  $\kappa_c$  is just a little lower than correlation coefficients of calculations using a  $\kappa_c$  conversion. As a result, the method of calculating  $N_{CCN}$  is insensitive to the uncertainty of the  $\kappa_c$  conversion.

In this study, the insensitivity of calculated  $N_{CCN}$  to  $\kappa_c$  conversion is partly due to the small variation of  $\kappa_f$  during the campaign. On one hand, the variation of  $\kappa_c$  can be quite large and cause non-ignorable deviations of calculated  $N_{CCN}$ . As previous studies of  $N_{CCN}$  measurement showed, the variation of  $\kappa_c$  is often small and a constant  $\kappa_c$  can be used to calculate  $N_{CCN}$  accurately (Andreae and Rosenfeld, 2008; Gunthe et al., 2009; Rose et al., 2010; Deng et al., 2013). Results in this study are similar to these previous studies. However, large variations of  $\kappa_c$  are also found in some other studies. In NCP, fluctuations of aerosol hygroscopicity during New Particle Formation events and soot emissions lead to significant deviations of calculated  $N_{CCN}$  from average aerosol hygroscopicity (Ma et al., 2016). On the other hand, the influence of  $\kappa_c$  cannot be ignored because the value of the average hygroscopicity is different in various regions during various periods. In summer of NCP, measured  $\kappa_f$  at sub-saturated conditions can reach up to 0.45 when inorganic compositions dominate in particles (Kuang et al., 2016). In this case, calculated  $N_{CCN}$  ignoring  $\kappa_c$  may be 10 times larger than measured  $N_{CCN}$ . To sum up, although the exact value of  $\kappa_c$  cannot be obtained from the measurement of the humidified nephelometer system, the influence of  $\kappa_c$  on  $N_{CCN}$  can be inferred and is found to be correct enough considering the convenience of this method. More data, especially in observations of more hygroscopic aerosol, is still needed to confirm this method.

324     4. Conclusions

325      $N_{CCN}$  is a key parameter of cloud microphysics and aerosol indirect radiative effect. Direct  
326     measurements of  $N_{CCN}$  are generally conducted under super-saturated conditions in cloud chambers,  
327     and are complex and costly. The aerosols of accumulation mode contribute most to both the aerosol  
328     scattering coefficient and the aerosol CCN activity. In view of this, it is possible to predict  $N_{CCN}$   
329     based on relationships between aerosol optical properties and the aerosol CCN activity. In this study,  
330     a new method is proposed to calculate  $N_{CCN}$  based on measurements of a humidified nephelometer  
331     system. In this method,  $N_{CCN}$  is derived from a look-up table which involves  $\sigma_{sp}$ , Å and  $\kappa_f$ , and  
332     the required three parameters can be obtained from a three-wavelength humidified nephelometer  
333     system.

334     Relationships between aerosol optical properties and aerosol CCN activity are investigated using  
335     datasets about aerosol PNSD measured during several campaigns in the North China Plain. The  
336     relationship between  $\sigma_{sp}$ , Å,  $\kappa_c$  and  $N_{CCN}$  is analyzed. It is found that the ratio between  $N_{CCN}$  and  
337      $\sigma_{sp}$ , referred to as  $AR_{sp}$ , is determined by  $\kappa_c$  and Å. In light of this, it is possible to calculate  $N_{CCN}$   
338     based only on measurements of a three-wavelength humidified nephelometer system which provides  
339     information about  $\sigma_{sp}$ , the hygroscopicity parameter  $\kappa$  and Å. However,  $\kappa$  derived from  
340     measurements of a humidified nephelometer system under sub-saturated conditions (termed as  $\kappa_f$ )  
341     differs from  $\kappa$  under super-saturated conditions which indicate CCN activity (termed as  $\kappa_c$ ). As a  
342     result, the conversion from  $\kappa_f$  to  $\kappa_c$  is needed. Based on previous studies of aerosol hygroscopicity  
343     and CCN activity, a simple conversion from  $\kappa_f$  to  $\kappa_c$  with a fixed difference (referred to as  $\Delta\kappa$ ) of  
344     0.2 is proposed. On the basis of this simple conversion, the method of  $N_{CCN}$  prediction based only on  
345     measurements of a humidified nephelometer system is achieved under conditions without sea salt  
346     aerosol, dust aerosol, externally mixed aerosol or aerosol near single source regions..

347     This method is validated with measurements from a humidified nephelometer system and a CCN  
348     counter in Gucheng in 2016. During the campaign, both  $N_{CCN}$  and  $\sigma_{sp}$  vary with the pollution  
349     conditions.  $AR_{sp}$  is around 5 and changes with Å and  $\kappa_f$ . The difference between  $\kappa_f$  and  $\kappa_c$ , was  
350      $0.2 \pm 0.1$ . The agreement between the calculated  $N_{CCN}$  and the measured  $N_{CCN}$  is achieved with

351 relative deviations less than 30%. Sensitivity of calculated  $N_{CCN}$  to conversions from  $\kappa_f$  to  $\kappa_c$  is  
352 studied by applying different kinds of conversions. Results show that calculated  $N_{CCN}$  varies little  
353 and is insensitive to the conversions, which confirms the robustness and applicability of this newly  
354 proposed method.

355 This study has connected aerosol optical properties with  $N_{CCN}$ , and also proposed a novel  
356 method to calculate  $N_{CCN}$  based only on measurements of a three-wavelength humidified  
357 nephelometer system. Due to the simple operation and stability of the humidified nephelometer  
358 system, this method will facilitate the real time monitoring of  $N_{CCN}$ , especially on aircrafts. In  
359 addition, measurements of the widely used CCN counter are limited to supersaturations higher than  
360 0.07. This method is more suitable for calculating  $N_{CCN}$  at lower supersaturations, thus is more  
361 applicable for ambient measurements of clouds and fogs in the atmosphere.

362

363 Acknowledgement

364 This work is supported by the National Natural Science Foundation of China (41590872,  
365 41375134 and 41505107).

366

367

## Reference

- 368 Andreae, M. O., and Rosenfeld, D.: Aerosol-cloud-precipitation interactions. Part 1. The nature and sources of cloud-active aerosols,  
 369 Earth-Science Reviews, 89, 13-41, 10.1016/j.earscirev.2008.03.001, 2008.
- 370 Andreae, M. O.: Correlation between cloud condensation nuclei concentration and aerosol optical thickness in remote and polluted  
 371 regions, Atmospheric Chemistry and Physics, 9, 543-556, 2009.
- 372 Brock, C. A., Wagner, N. L., Anderson, B. E., Attwood, A. R., Beyersdorf, A., Campuzano-Jost, P., Carlton, A. G., Day, D. A., Diskin, G. S.,  
 373 Gordon, T. D., Jimenez, J. L., Lack, D. A., Liao, J., Markovic, M. Z., Middlebrook, A. M., Ng, N. L., Perring, A. E., Richardson, M. S.,  
 374 Schwarz, J. P., Washenfelder, R. A., Welti, A., Xu, L., Ziembka, L. D., and Murphy, D. M.: Aerosol optical properties in the southeastern  
 375 United States in summer – Part 1: Hygroscopic growth, Atmos. Chem. Phys., 16, 4987-5007, 10.5194/acp-16-4987-2016, 2016.
- 376 Chen, J., Zhao, C. S., Ma, N., and Yan, P.: Aerosol hygroscopicity parameter derived from the light scattering enhancement factor  
 377 measurements in the North China Plain, Atmos. Chem. Phys., 14, 8105-8118, 10.5194/acp-14-8105-2014, 2014.
- 378 Cheng, Y. F., Wiedensohler, A., Eichler, H., Su, H., Gnauk, T., Bruegmann, E., Herrmann, H., Heintzenberg, J., Slanina, J., Tuch, T., Hu,  
 379 M., and Zhang, Y. H.: Aerosol optical properties and related chemical apportionment at Xinken in Pearl River Delta of China, Atmos.  
 380 Environ., 42, 6351-6372, 10.1016/j.atmosenv.2008.02.034, 2008.
- 381 Covert, D. S., Charlson, R., and Ahlquist, N.: A study of the relationship of chemical composition and humidity to light scattering by  
 382 aerosols, Journal of applied meteorology, 11, 968-976, 1972.
- 383 Cubison, M. J., Ervens, B., Feingold, G., Docherty, K. S., Ulbrich, I. M., Shields, L., Prather, K., Hering, S., and Jimenez, J. L.: The  
 384 influence of chemical composition and mixing state of Los Angeles urban aerosol on CCN number and cloud properties, Atmospheric  
 385 Chemistry and Physics, 8, 5649-5667, 2008.
- 386 Deng, Z. Z., Zhao, C. S., Ma, N., Liu, P. F., Ran, L., Xu, W. Y., Chen, J., Liang, Z., Liang, S., Huang, M. Y., Ma, X. C., Zhang, Q., Quan, J. N.,  
 387 Yan, P., Henning, S., Mildenberger, K., Sommerhage, E., Schäfer, M., Stratmann, F., and Wiedensohler, A.: Size-resolved and bulk  
 388 activation properties of aerosols in the North China Plain, Atmos. Chem. Phys., 11, 3835-3846, 10.5194/acp-11-3835-2011, 2011.
- 389 Deng, Z. Z., Zhao, C. S., Ma, N., Ran, L., Zhou, G. Q., Lu, D. R., and Zhou, X. J.: An examination of parameterizations for the CCN  
 390 number concentration based on in situ measurements of aerosol activation properties in the North China Plain, Atmos. Chem. Phys.,  
 391 13, 6227-6237, 10.5194/acp-13-6227-2013, 2013.
- 392 Dusek, U., Frank, G., Hildebrandt, L., Curtius, J., Schneider, J., Walter, S., Chand, D., Drewnick, F., Hings, S., and Jung, D.: Size matters  
 393 more than chemistry for cloud-nucleating ability of aerosol particles, Science, 312, 1375-1378, 2006.
- 394 Ervens, B., Cubison, M., Andrews, E., Feingold, G., Ogren, J. A., Jimenez, J. L., DeCarlo, P., and Nenes, A.: Prediction of cloud  
 395 condensation nucleus number concentration using measurements of aerosol size distributions and composition and light scattering  
 396 enhancement due to humidity, Journal of Geophysical Research: Atmospheres, 112, n/a-n/a, 10.1029/2006jd007426, 2007.
- 397 Ervens, B., Cubison, M. J., Andrews, E., Feingold, G., Ogren, J. A., Jimenez, J. L., Quinn, P. K., Bates, T. S., Wang, J., Zhang, Q., Coe, H.,  
 398 Flynn, M., and Allan, J. D.: CCN predictions using simplified assumptions of organic aerosol composition and mixing state: a synthesis  
 399 from six different locations, Atmospheric Chemistry and Physics, 10, 4795-4807, 10.5194/acp-10-4795-2010, 2010.
- 400 Gasso, S., and Hegg, D. A.: On the retrieval of columnar aerosol mass and CCN concentration by MODIS, J. Geophys. Res.-Atmos., 108,  
 401 4010  
 402 10.1029/2002jd002382, 2003.
- 403 Ghan, S. J., and Collins, D. R.: Use of in situ data to test a Raman lidar-based cloud condensation nuclei remote sensing method,  
 404 Journal of Atmospheric and Oceanic Technology, 21, 387-394, 10.1175/1520-0426(2004)021<0387:uoisdt>2.0.co;2, 2004.
- 405 Ghan, S. J., Rissman, T. A., Elleman, R., Ferrare, R. A., Turner, D., Flynn, C., Wang, J., Ogren, J., Hudson, J., Jonsson, H. H., VanReken, T.,  
 406 Flagan, R. C., and Seinfeld, J. H.: Use of in situ cloud condensation nuclei, extinction, and aerosol size distribution measurements to  
 407 test a method for retrieving cloud condensation nuclei profiles from surface measurements, J. Geophys. Res.-Atmos., 111, D05s10  
 408 10.1029/2004jd005752, 2006.
- 409 Gunthe, S. S., King, S. M., Rose, D., Chen, Q., Roldin, P., Farmer, D. K., Jimenez, J. L., Artaxo, P., Andreae, M. O., Martin, S. T., and Poschl,  
 410 U.: Cloud condensation nuclei in pristine tropical rainforest air of Amazonia: size-resolved measurements and modeling of

411 atmospheric aerosol composition and CCN activity, *Atmospheric Chemistry and Physics*, 9, 7551-7575, 2009.  
412 Hudson, J. G.: AN INSTANTANEOUS CCN SPECTROMETER, *Journal of Atmospheric and Oceanic Technology*, 6, 1055-1065,  
413 10.1175/1520-0426(1989)006<1055:aics>2.0.co;2, 1989.  
414 Jefferson, A.: Empirical estimates of CCN from aerosol optical properties at four remote sites, *Atmos. Chem. Phys.*, 10, 6855-6861,  
415 10.5194/acp-10-6855-2010, 2010.  
416 Köhler, H.: The nucleus in and the growth of hygroscopic droplets, *Transactions of the Faraday Society*, 32, 1152-1161, 1936.  
417 Kapustin, V. N., Clarke, A. D., Shinozuka, Y., Howell, S., Brekhovskikh, V., Nakajima, T., and Higurashi, A.: On the determination of a  
418 cloud condensation nuclei from satellite: Challenges and possibilities, *J. Geophys. Res.-Atmos.*, 111, D04202  
419 10.1029/2004jd005527, 2006.  
420 Kreidenweis, S. M., and Asa-Awuku, A.: 5.13 - Aerosol Hygroscopicity: Particle Water Content and Its Role in Atmospheric Processes  
421 A2 - Holland, Heinrich D, in: *Treatise on Geochemistry (Second Edition)*, edited by: Turekian, K. K., Elsevier, Oxford, 331-361, 2014.  
422 Kuang, Y., Zhao, C. S., Ma, N., Liu, H. J., Bian, Y. X., Tao, J. C., and Hu, M.: Deliquescent phenomena of ambient aerosols on the North  
423 China Plain, *Geophys. Res. Lett.*, n/a-n/a, 10.1002/2016gl070273, 2016.  
424 Kuang, Y., Zhao, C., Tao, J., Bian, Y., Ma, N., and Zhao, G.: A novel method to derive the aerosol hygroscopicity parameter based only  
425 on measurements from a humidified nephelometer system, *Atmos. Chem. Phys. Discuss.*, 2017, 1-25, 10.5194/acp-2016-1066, 2017a.  
426 Kuang, Y., Zhao, C. S., Tao, J. C., Bian, Y. X., Ma, N., and Zhao, G.: A novel method for deriving the aerosol hygroscopicity parameter  
427 based only on measurements from a humidified nephelometer system, *Atmospheric Chemistry and Physics*, 17, 6651-6662,  
428 10.5194/acp-17-6651-2017, 2017b.  
429 Lance, S., Nenes, A., Medina, J., and Smith, J.: Mapping the operation of the DMT continuous flow CCN counter, *Aerosol science and*  
430 *technology*, 40, 242-254, 2006.  
431 Lathem, T. L., and Nenes, A.: Water Vapor Depletion in the DMT Continuous-Flow CCN Chamber: Effects on Supersaturation and  
432 Droplet Growth, *Aerosol science and technology*, 45, 604-615, 10.1080/02786826.2010.551146, 2011.  
433 Liu, H. J., Zhao, C. S., Nekat, B., Ma, N., Wiedensohler, A., van Pinxteren, D., Spindler, G., Müller, K., and Herrmann, H.: Aerosol  
434 hygroscopicity derived from size-segregated chemical composition and its parameterization in the North China Plain, *Atmos. Chem.*  
435 *Phys.*, 14, 2525-2539, 10.5194/acp-14-2525-2014, 2014.  
436 Liu, J. J., and Li, Z. Q.: Estimation of cloud condensation nuclei concentration from aerosol optical quantities: influential factors and  
437 uncertainties, *Atmospheric Chemistry and Physics*, 14, 471-483, 10.5194/acp-14-471-2014, 2014.  
438 Ma, N., Zhao, C., Nowak, A., Müller, T., Pfeifer, S., Cheng, Y., Deng, Z., Liu, P., Xu, W., and Ran, L.: Aerosol optical properties in the  
439 North China Plain during HaChi campaign: an in-situ optical closure study, *Atmos. Chem. Phys.*, 11, 5959-5973, 2011.  
440 Ma, N., Zhao, C., Tao, J., Wu, Z., Kecorius, S., Wang, Z., Größ, J., Liu, H., Bian, Y., Kuang, Y., Teich, M., Spindler, G., Müller, K., van  
441 Pinxteren, D., Herrmann, H., Hu, M., and Wiedensohler, A.: Variation of CCN activity during new particle formation events in the  
442 North China Plain, *Atmos. Chem. Phys.*, 16, 8593-8607, 10.5194/acp-16-8593-2016, 2016.  
443 McMeeking, G. R., Morgan, W. T., Flynn, M., Highwood, E. J., Turnbull, K., Haywood, J., and Coe, H.: Black carbon aerosol mixing state,  
444 organic aerosols and aerosol optical properties over the United Kingdom, *Atmos. Chem. Phys.*, 11, 9037-9052,  
445 10.5194/acp-11-9037-2011, 2011.  
446 Moteki, N., and Kondo, Y.: Effects of Mixing State on Black Carbon Measurements by Laser-Induced Incandescence, *Aerosol science*  
447 and *technology*, 41, 398-417, 10.1080/02786820701199728, 2007.  
448 Nenes, A., Chuang, P. Y., Flagan, R. C., and Seinfeld, J. H.: A theoretical analysis of cloud condensation nucleus (CCN) instruments, *J.*  
449 *Geophys. Res.-Atmos.*, 106, 3449-3474, 10.1029/2000jd900614, 2001.  
450 Petters, M. D., and Kreidenweis, S. M.: A single parameter representation of hygroscopic growth and cloud condensation nucleus  
451 activity, *Atmospheric Chemistry and Physics*, 7, 1961-1971, 2007.  
452 Roberts, G., and Nenes, A.: A continuous-flow streamwise thermal-gradient CCN chamber for atmospheric measurements, *Aerosol*  
453 *science and technology*, 39, 206-221, 2005.  
454 Rose, D., Gunthe, S., Mikhailov, E., Frank, G., Dusek, U., Andreae, M., and Pöschl, U.: Calibration and measurement uncertainties of a

455 continuous-flow cloud condensation nuclei counter (DMT-CCNC): CCN activation of ammonium sulfate and sodium chloride aerosol  
456 particles in theory and experiment, *Atmospheric Chemistry and Physics*, 8, 1153-1179, 2008.

457 Rose, D., Nowak, A., Achtert, P., Wiedensohler, A., Hu, M., Shao, M., Zhang, Y., Andreae, M. O., and Poschl, U.: Cloud condensation  
458 nuclei in polluted air and biomass burning smoke near the mega-city Guangzhou, China - Part 1: Size-resolved measurements and  
459 implications for the modeling of aerosol particle hygroscopicity and CCN activity, *Atmospheric Chemistry and Physics*, 10, 3365-3383,  
460 2010.

461 Shinozuka, Y., Clarke, A. D., Nenes, A., Jefferson, A., Wood, R., McNaughton, C. S., Ström, J., Tunved, P., Redemann, J., Thornhill, K. L.,  
462 Moore, R. H., Lathem, T. L., Lin, J. J., and Yoon, Y. J.: The relationship between cloud condensation nuclei (CCN) concentration and light  
463 extinction of dried particles: indications of underlying aerosol processes and implications for satellite-based CCN estimates, *Atmos.  
464 Chem. Phys.*, 15, 7585-7604, 10.5194/acp-15-7585-2015, 2015.

465 Titos, G., Cazorla, A., Zieger, P., Andrews, E., Lyamani, H., Granados-Muñoz, M. J., Olmo, F. J., and Alados-Arboledas, L.: Effect of  
466 hygroscopic growth on the aerosol light-scattering coefficient: A review of measurements, techniques and error sources, *Atmos.  
467 Environ.*, 141, 494-507, <http://dx.doi.org/10.1016/j.atmosenv.2016.07.021>, 2016.

468 Wex, H., McFiggans, G., Henning, S., and Stratmann, F.: Influence of the external mixing state of atmospheric aerosol on derived CCN  
469 number concentrations, *Geophys. Res. Lett.*, 37, L10805  
470 10.1029/2010gl043337, 2010.

471 Whitehead, J. D., Irwin, M., Allan, J. D., Good, N., and McFiggans, G.: A meta-analysis of particle water uptake reconciliation studies,  
472 *Atmos. Chem. Phys.*, 14, 11833-11841, 10.5194/acp-14-11833-2014, 2014.

473 Wu, Z. J., Poulain, L., Henning, S., Dieckmann, K., Birmili, W., Merkel, M., van Pinxteren, D., Spindler, G., Mueller, K., Stratmann, F.,  
474 Herrmann, H., and Wiedensohler, A.: Relating particle hygroscopicity and CCN activity to chemical composition during the HCCT-2010  
475 field campaign, *Atmospheric Chemistry and Physics*, 13, 7983-7996, 10.5194/acp-13-7983-2013, 2013.

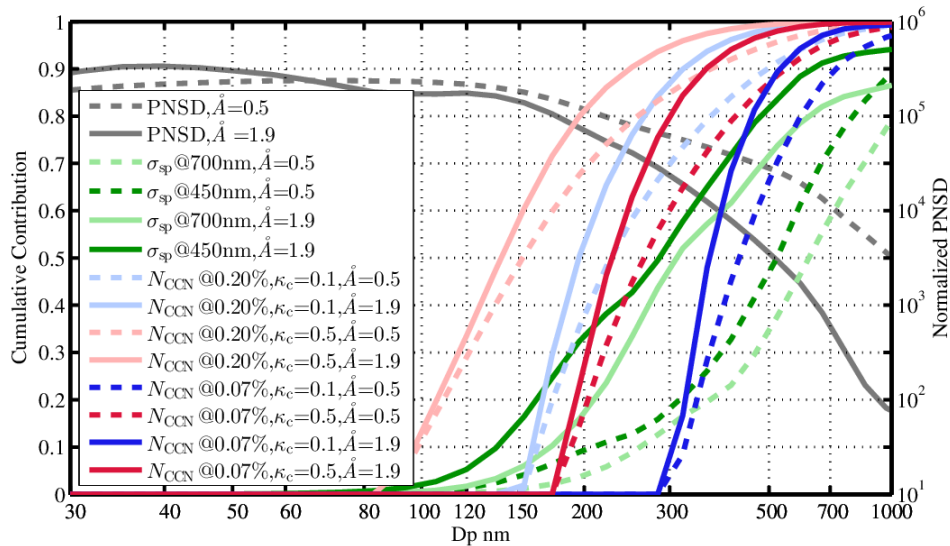
476 Renbaum-Wolff, L., M. Song, et al. (2016). "Observations and implications of liquid–liquid phase separation at high relative  
477 humidities in secondary organic material produced by  $\alpha$ -pinene ozonolysis without inorganic salts." *Atmos. Chem. Phys.*  
478 16(12): 7969-7979.

479 Irwin, M., N. Good, et al. (2010). "Reconciliation of measurements of hygroscopic growth and critical supersaturation of  
480 aerosol particles in central Germany." *Atmos. Chem. Phys.* **10**(23): 11737-11752.

481 Good, N., D. O. Topping, et al. (2010). "Consistency between parameterisations of aerosol hygroscopicity and CCN activity  
482 during the RHaMBLe discovery cruise." *Atmospheric Chemistry and Physics* **10**(7): 3189-3203.

483

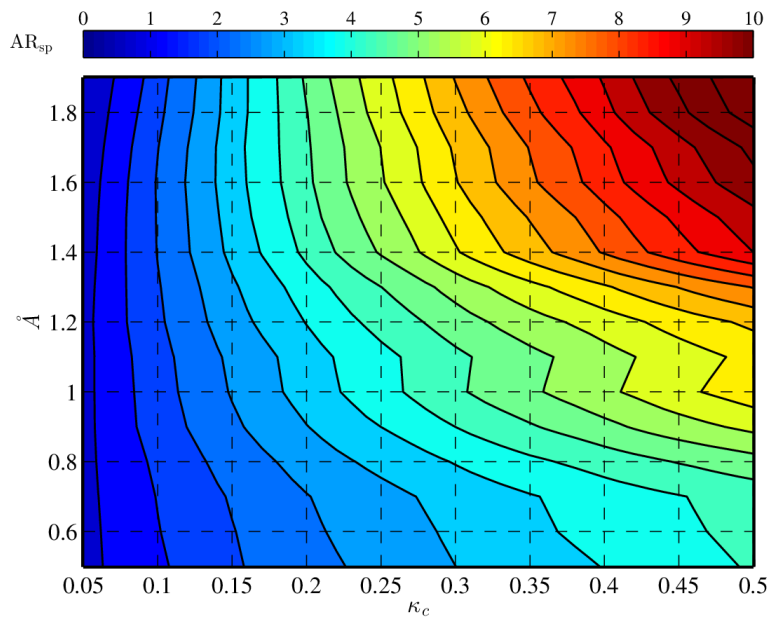
484



485

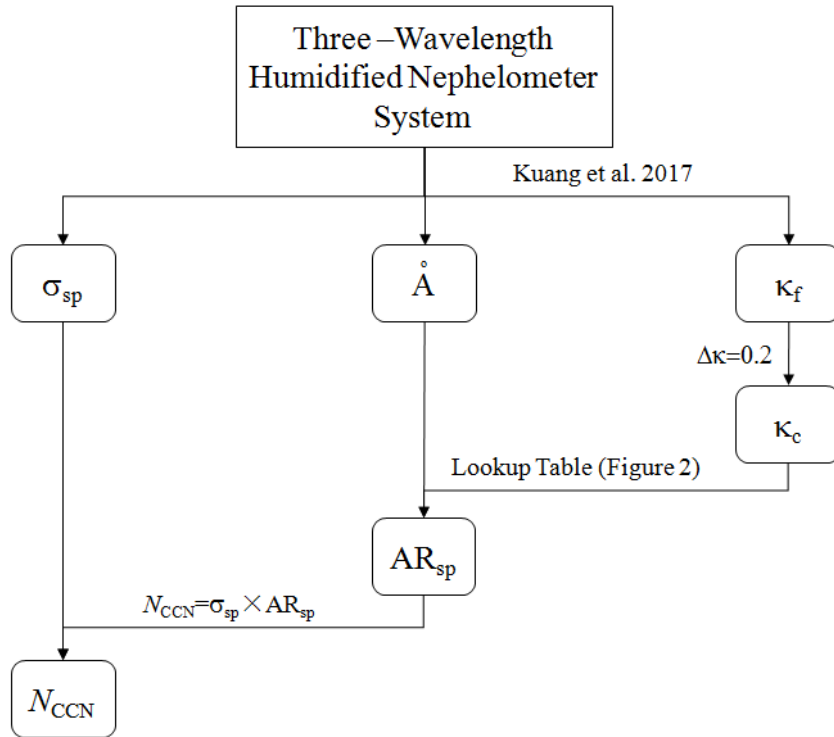
486 Figure 1.

487 Aerosol PNSD (black lines), the cumulative contribution of  $\sigma_{\text{sp}}$  at wavelength of 450nm and 700nm  
 488 (dark green lines and light green lines, respectively), the cumulative contribution of  $N_{\text{CCN}}$  at  
 489 supersaturation of 0.07% (dark red and dark blue lines) and the cumulative contribution of  $N_{\text{CCN}}$  at  
 490 supersaturation of 0.20% (light red and light blue lines) based on measurement in several campaigns  
 491 in the North China Plain. Solid lines and dashed lines indicate  $\text{\AA}$  of 1.9 and 0.5, respectively. Blue  
 492 lines and red lines indicate  $\kappa_c$  of 0.1 and 0.5, respectively.



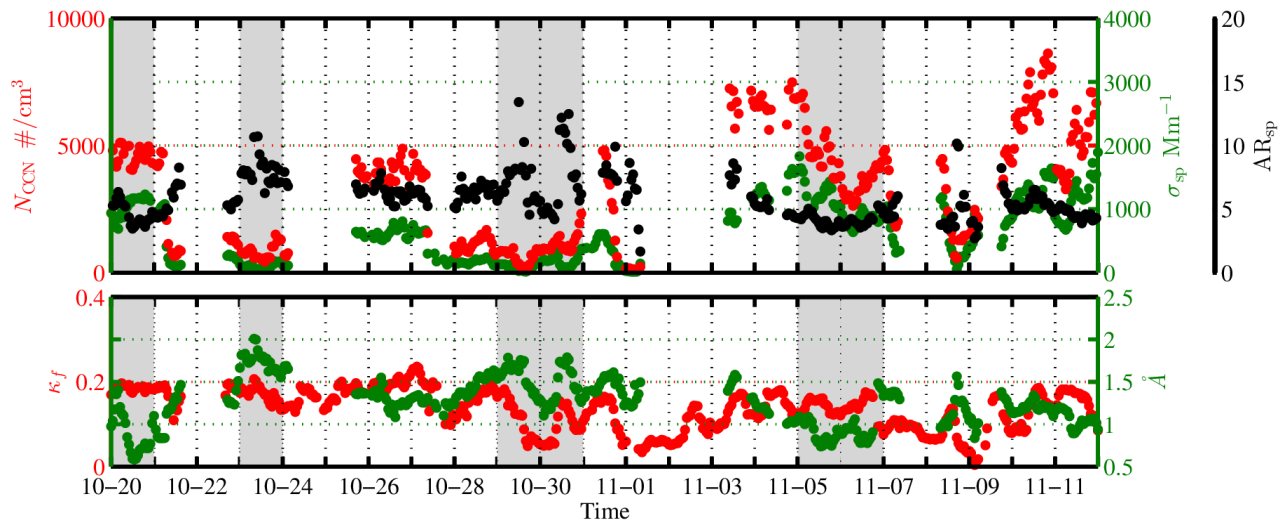
493  
494 Figure 2.

495 Colors represent  $AR_{sp}$  (calculated as  $AR_{sp} = \frac{N_{CCN}}{\sigma_{sp}}$  at 450nm wavelength and 0.07% supersaturation)  
496 with different PNSDs (classified by  $\text{Å}$  values) and different  $\kappa_c$ .

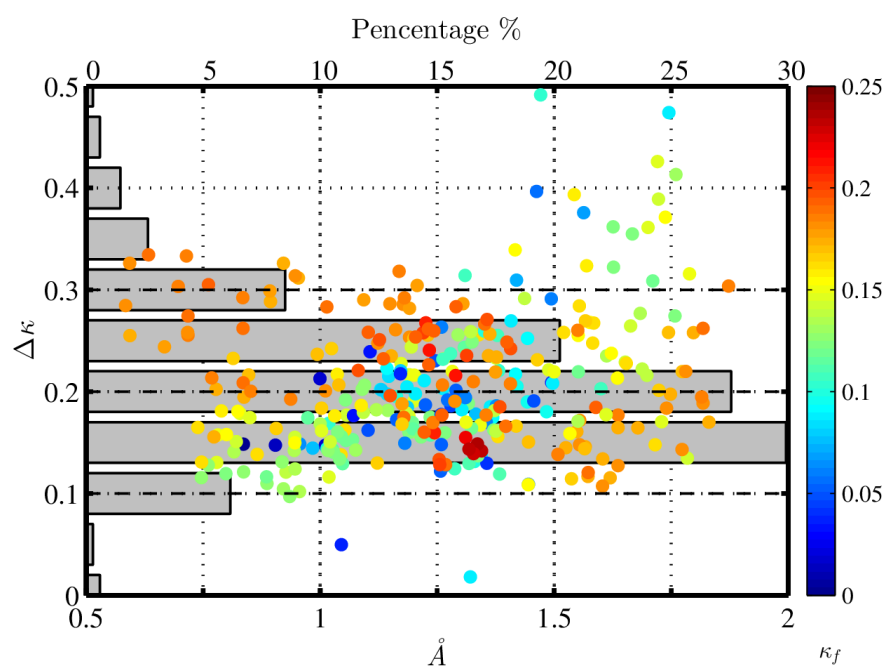


497  
498 Figure 3.

499 The schematic chart of the  $N_{\text{CCN}}$  prediction based on measurements of a humidified nephelometer  
500 system.



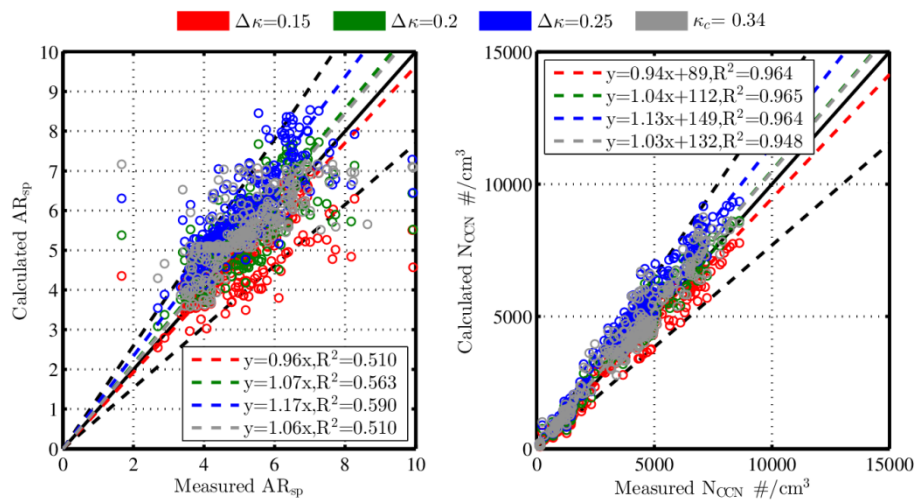
501  
502 Figure 4.  
503 Overview of measurements in Gucheng in 2016. Upper plot: time series of  $N_{\text{CCN}}$  at the  
504 supersaturation of 0.07% (red dots),  $\sigma_{\text{sp}}$  at the wavelength of 50nm (green dots) and their ratios  
505 (black dots), referred to as  $\text{AR}_{\text{sp}}$ . Lower plot: time series of  $\kappa_f$  (red dots) and  $\text{\AA}$  (green dots). The  
506 grey bars are periods when the sensitivity of  $\text{AR}_{\text{sp}}$  to  $\kappa_c$  is notable.



507

508 Figure 5.

509 Differences between  $\kappa_c$  and  $\kappa_f$ , referred to as  $\Delta\kappa$ , with Å (positions of dots) and  $\kappa_f$  (colors of  
 510 dots). Bars represent percentages of  $\Delta\kappa$  within different ranges.



512 Figure 6.

513 Left plot: comparisons of calculated AR<sub>sp</sub> and measured AR<sub>sp</sub> with different conversions of  $\kappa_c$  from  
 514  $\kappa_f$ . Right plot: regressions of calculated  $N_{CCN}$  and measured  $N_{CCN}$  with different conversions of  $\kappa_c$   
 515 from  $\kappa_f$ .

Campaign	Air mass	Parameter	Caveats	Results	Reference
ICARTT <sup>1</sup> in the north eastern USA and Canada	Polluted air mass	fRH and PNSD	Calculate $N_{CCN}$ with aerosol hygroscopicity contrained by f(RH) and PNSD.	Predict $N_{CCN}$ at SS > 0.3% with a 0.9 R <sup>2</sup> .	Ervens et al., 2007
HaChi <sup>2</sup> on the North China Plain	Aged continental air mass	PNSD and fRH	Similar to Ervens et al., 2007.  Calculate $N_{CCN}$ with the hygroscopicity parameter contrained by f(RH) and PNSD.	Slopes around 1 and R <sup>2</sup> around 0.9.	Chen et al., 2014

TARFOX <sup>3</sup> Atlantic seaboard and ACE-2 <sup>4</sup>	Polluted air mass	Retrieved aerosol volume from remote sensing	Predict $N_{CCN}$ from aerosol volumes with empirical number-to-volume concentration ratio	Overestimate up to 5 times	Gasso and Hegg, 2003
ACE-2 in northeastern Atlantic	Diverse air mass	Backscatter or extinction profile. CCN at the surface.	Retrieve $N_{CCN}$ profile from backscatter (or extinction) vertical profile assuming their ratios are the same to the ratio at surface, which can be calculated by backscatter (or extinction) and $N_{CCN}$ measured at the surface	Predict $N_{CCN}$ on most days for 0.1% SS and on 20%–40% of the days at 1% SS.	Ghan and Collins, 2004
ARM <sup>5</sup> Climate Research Facility central site at the Southern Great Plains	Continental air mass	Backscatter (or extinction) and RH profile. fRH and CCN at surface	Same as Ghan and Collins, 2004.	Explains CCN variance for 25%–63% of all measurements at high supersaturations	Ghan et al., 2006
TRACE-P <sup>6</sup> and ACE-Asia <sup>7</sup>	Asian outflow over the western Pacific	Aerosol Index (AI, the product of ambient light extinction and Å)	Predict $N_{CCN}$ based on empirical relationship between AI and $N_{CCN}$	AI relate well to CCN only with suitably stratified data	Kapustin et al., 2006
Multiple measurements	Diverse air mass	AERONET aerosol optical thickness (AOT)	Predict $N_{CCN}$ based on empirical relationship between AOT and $N_{CCN}$ as a power law	Predict $N_{CCN}$ at SS > 0.3% with a 0.88 $R^2$ , but have a factor-of-four range of $N_{CCN}$ at a given AOT	Andreae, 2009
Four ARM sites	Polluted air mass	SSA, backscatter fraction and $\sigma_{sp}$	Estimate $N_{CCN}$ from fitting parameters for the $N_{CCN}$ activity spectra, which can be calculate based on their empirical relationships with	Predict $N_{CCN}$ with slopes around 0.9 and $R^2$ around 0.6.	Jefferson, 2010

aerosol optical properties.

Multiple ARM sites around the world	Diverse air mass	RH, fRH, SSA, AOT and $\sigma_{sp}$	Calculate $N_{CCN}$ with $\sigma_{sp}$ (or AOT) based on their empirical relationship, whose impact RH, fRH and SSA.	Achieve the best results by using $\sigma_{sp}$ and SSA. Weakly affect on the $\sigma_{sp}$ - $N_{CCN}$ relationship by fRH. Deteriorate $N_{CCN}$ -AOT relationship with increasing RH	Liu and Li, 2014
Multiple ARM sites around the world	Diverse air mass not dominated by dust	$\text{\AA}$ and extinction coefficient	Calculate $N_{CCN}$ with light extinction based on their emperical relationship.	Deviate typically within a factor of 2.0.	Shinozuka et al., 2015

- 518 Tabel 1.  
519 Review of studies that have used aerosol optical parameters to infer  $N_{CCN}$ .  
520 <sup>1</sup> International Consortium for Atmospheric Research on Transport and Transformation.  
521 <sup>2</sup> Haze in China.  
522 <sup>3</sup> Troposphere Aerosol Radiative Forcing Experiment.  
523 <sup>4</sup> Second Aerosol Characterization Experiment.  
524 <sup>5</sup> Atmospheric Radiation Measurement.  
525 <sup>6</sup> Transport and Chemical Evolution over the Pacific.  
526 <sup>7</sup> Aerosol Characterization Experiment–Asia.  
527